

DIAGNOSTIC MODEL OF 3-D CIRCULATION IN THE ARABIAN SEA AND WESTERN EQUATORIAL INDIAN OCEAN: RESULTS OF MONTHLY MEAN SEA SURFACE TOPOGRAPHY

N BAHULAYAN¹ AND C SHAJI²

1. *Physical Oceanography Division, National Institute of Oceanography, Dona Paula, Goa-403 004, India*
2. *Centre for Atmospheric Sciences, Indian Institute of Technology, Hauz Khas, New Delhi-110 016, India*

(Received 08 November 1993; Finally Revised 11 September 1995; Accepted 23 March 1996)

A three-dimensional diagnostic model has been developed to compute the monthly mean circulation and sea surface topography in the Western Tropical Indian Ocean north of 20°S and west of 80°E. The diagnostic model equations are the basic ocean hydrodynamic equations of momentum, hydrostatics, continuity and sea surface topography. There are total five equations in five unknowns. While the hydrodynamic equations of momentum, hydrostatics and continuity are solved by a leap-frog numerical scheme, the sea surface topography equation is solved by successive over-relaxation technique. Model has 18 levels in the vertical with a maximum depth of 900 meters, a resolution of 1° in the latitude and longitude directions and is forced by climatologically averaged monthly mean winds temperature and salinity data (density anomaly).

Model computed results of sea surface topography for all the 12 months and its associated circulation are analysed and presented in this paper. Model reproduced realistically the sea surface topography for all 12 months. The computed sea surface topography and its associated circulation were compared with available observations on currents and both found to agree fairly well. In the southern tropical Indian Ocean south of 10°S latitude, the computed sea surface topography patterns do not show much variability from month to month due to the absence of seasonal variability in the wind field. However, monthly variability of sea surface topography was noticed in the entire model area north of 10°S latitude.

Key Words: 3-Dimensional; Diagnostic Model; Leap-frog; Sea Surface Topography; Circulation; Thermohaline Forcing

Introduction

The large scale air-sea interaction processes on monthly, seasonal and intra-seasonal scales in the Arabian Sea are mainly controlled by basin scale 3-dimensional circulation that generates temperature and salinity inhomogeneities in the Sea and modifies the heat budget parameters at the air-sea interface. One of the unique oceanographic characteristics of Arabian Sea is its intense warming and cooling during the premonsoon and monsoon seasons respectively, which have a direct bearing on the monsoonal atmospheric circulation. To understand the dynamics that control the temperature and salinity variability and to predict the warming and cooling processes in the Arabian Sea, it is first essential to compute mathematically the monthly mean 3-dimensional circulation which would serve as initial conditions in prognostic models of ocean circulation.

Three-dimensional circulation on basin scales is always computed from indirect observations of oceanic properties, especially observations on tempera-

ture and salinity. In the early 1950's dynamic method was commonly used to compute density driven circulation in the sea. This method has a number of drawbacks: it computes only the relative currents under the assumption that flow velocity is zero at some lower levels. In the real ocean, the vertical profile of gradient flow may behave quite arbitrarily: at some depth, the flow direction changes sign, while at some depth it decreases slowly or increases abruptly. There is no zero velocity level in the real ocean that could be taken as reference level. In addition, the dynamic method does not take into account the direct effect of tangential wind stress and bottom topography. The upper level circulation in the ocean is mainly controlled by wind stress forcing and therefore it is necessary to develop alternate methods for the computation of 3-d circulation that take into consideration wind stress, thermohaline forcing and bottom topography. One of the methods normally used to study 3-d circulation in the ocean, considering wind field and thermohaline forcing, is diagnostic method. In a diagnostic model, primitive equations of momentum, hydrostatics and continuity are integrated with appropriate boundary and initial conditions using observed density and wind stress forcing parameters. Since density is directly imposed on the model from observations of temperature and salinity, there is no need to include the equation of state and turbulent diffusion equations of heat and salt in the diagnostic model. Equation of state is used to derive the density field and the density is kept constant throughout the model integration in diagnostic models. Pioneering works in the field of diagnostic modelling were carried out by Sarkisyan and his co-workers in the erstwhile Soviet Union¹⁻³. There have been many studies on the modelling of circulation in the Arabian Sea. Most of these studies were aimed at studying the dynamics of Somali current that flows northeastward and southwestward along the coast of Somalia during the southwest and northeast monsoons respectively⁴⁻⁸. The dynamics of Somali current were explained theoretically using layer models of varying complexities. Several such layer models of Indian ocean circulation exist in oceanographic literature⁹⁻¹⁴. There is hardly any information on the monthly mean climatological circulation in the subsurface layers of the Arabian Sea which is mainly controlled by the vertical variation in the density field apart from wind stress forcing.

The main objective of this paper is to develop an 18 level diagnostic model of circulation that will consider both wind stress and thermohaline forcing at different levels to determine the large scale monthly mean circulation in the Western tropical Indian ocean. Details of diagnostic model, its boundary and initial conditions, numerical solution procedure, computational results of sea surface topography for all the 12 months and its associated circulation features and a comparison of model results with available information on observed currents are presented in this paper.

Model Equations

For our model, the basic hydrodynamical equations that govern the large scale 3-dimensional flows in spherical co-ordinate system were taken from Gill¹⁵. Scale analysis of the governing equations shows that nonlinear and friction

terms have the same order of magnitude and both play a major role in the dynamics of circulation in the equatorial regions where geostrophy fails. The sign convention used in this paper is different from the standard sign convention used in oceanography. We use a coordinate system wherein the longitude (λ), the co-latitude (θ), and vertical coordinate (z) increase towards east, south and downward directions respectively. Assuming approximations of Boussinesq, hydrostatics and incompressibility, the final model equations are written as follows:

$$\frac{\partial u}{\partial t} + Au + lv + \cot \theta \frac{uv}{R} = -\frac{1}{\rho_0 R \sin \theta} \frac{\partial p}{\partial \lambda} + F^\lambda, \quad \dots (1)$$

$$\frac{\partial v}{\partial t} + Av - lu - \cos \theta \frac{u^2}{R} = -\frac{1}{\rho_0 R} \frac{\partial p}{\partial \theta} + F^\theta, \quad \dots (2)$$

$$\frac{\partial p}{\partial z} = g\rho \quad \dots (3)$$

and

$$\frac{1}{R \sin \theta} \left[\frac{\partial u}{\partial \lambda} + \frac{\partial (v \sin \theta)}{\partial \theta} \right] + \frac{\partial w}{\partial z} = 0, \quad \dots (4)$$

where

θ = co-latitude = $90 - \phi$, ϕ is the latitude.

u, v, w = the velocity components along the east (λ), south (θ) and downward (z) directions respectively.

p = hydrostatic pressure.

ρ = density of sea water.

ρ_0 = average density of sea water.

R = radius of the Earth.

l = $2\Omega \cos \theta$.

Ω = angular velocity of Earth's rotation.

$$Af = \frac{1}{R \sin \theta} \left[\frac{\partial (uf)}{\partial \lambda} + v \frac{\partial (f \sin \theta)}{\partial \theta} \right] + \frac{\partial (wf)}{\partial z},$$

$$F^\lambda = \frac{\partial (v \partial u / \partial z)}{\partial z} + \mu \left[\Delta u - \frac{1}{R^2 \sin^2 \theta} \left(u - 2 \frac{\partial (v \cos \theta)}{\partial \lambda} \right) \right],$$

$$F^\theta = \frac{\partial (v \partial v / \partial z)}{\partial z} + \mu \left[\Delta v - \frac{v}{R^2 \sin^2 \theta} + \frac{2 \cos \theta}{R^2 \sin^2 \theta} \frac{\partial u}{\partial \lambda} \right]$$

and

$$\Delta f = \frac{1}{R^2 \sin^2 \theta} \frac{\partial^2 f}{\partial \lambda^2} + \frac{1}{R^2 \sin \theta} \frac{\partial(\sin \theta \partial f / \partial \theta)}{\partial \theta},$$

μ, ν —horizontal and vertical turbulent mixing coefficients respectively.

The density of sea water, ρ , can be written as the sum of the average density ρ_0 and density anomaly $\rho'(x, y, z)$. Integrating the hydrostatic eq. (3) in the vertical from free surface to depth, the expression for hydrostatic pressure is obtained as follows:

$$P = \rho_0 g \xi + g \int_0^z \rho' dz, \quad \dots (5)$$

where ' ξ ' is the sea topography which is otherwise called sea level. The first term on the right hand side of eq. (5) represents the hydrostatic pressure due to free surface elevation. While integrating the hydrostatic eq. (3) in the vertical from the surface to depth, the hydrostatic pressure due to average density ρ_0 is neglected and only the hydrostatic pressure due to density anomaly resulting from variations in temperature and salinity will be retained. In fact, the density anomaly ρ' and the actual density ρ as defined in eq. (3) are one and the same. The mean density ρ_0 has been assigned a value equal to 1.0 gm/cm³. The density anomaly was calculated using the formula recommended by UNESCO, the details of which are given in the text book by Marchuk and Sarkisyan³. We first calculated σ_t (sigma- t) from observations of temperature and salinity and then density anomaly ρ' was calculated using the standard relation that connects sigma- t and density. The pressure gradient terms in the momentum equations (1) and (2) are computed using eq. (5). The unknowns in the model equations are the velocity components (u, v, w), pressure (p) and sea level (ξ). There are five unknowns in four equations (eqns 1, 2, 4 and 5). The density of sea water which is imposed on the model from observations of temperature and salinity is not a prognostic variable in diagnostic circulation models. It is necessary to derive an expression for sea surface topography (sea level) to have a closed system of five equations in five unknowns. A brief description of the procedure to derive sea surface topography equation and the final sea surface topography equation are given on Page Nos. 332-333.

Boundary Conditions

The model area lies between the latitudinal belt 30°N-20°S and longitudinal belt 35°E-80°E (Fig. 1). The entire southern boundary and part of eastern boundary of the model are open boundaries where appropriate open boundary conditions for velocity or volume flux are to be specified. The western, northern and part of eastern boundaries of the model are closed boundaries.

At the surface ($z=0$), a rigid lid boundary condition for vertical velocity is employed. Specification of rigid lid boundary condition at surface will eliminate short period surface gravitational waves from the solution and will also enable us to use larger time steps of integration. However, large scale waves such as

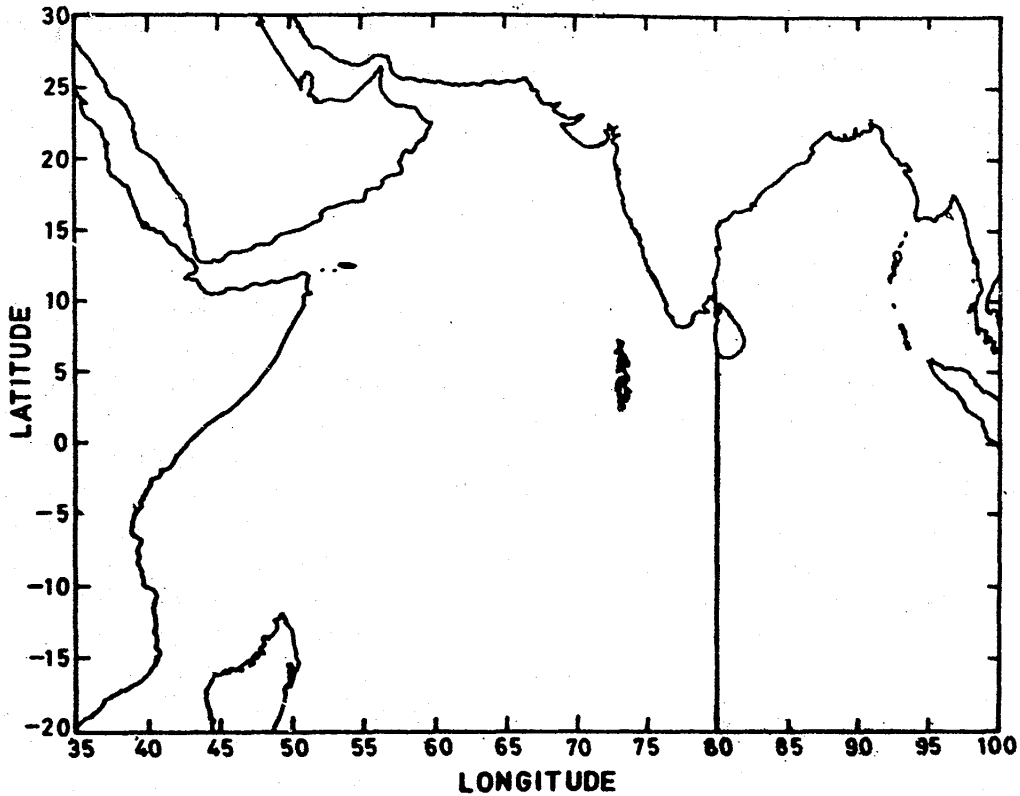


Fig 1 Geometry of the model basin. The entire southern boundary along 20°S latitude and part of eastern boundary along 80°E longitude are open boundaries.

Rossby and Kelvin are retained in the solution. The resultant wind stress at the sea surface is expressed in terms of the gradient of velocity in the vertical multiplied by the vertical turbulent mixing coefficient and mean density of sea water. Thus, the boundary conditions at the surface are:

$$\left. \begin{aligned} -\tau_\lambda &= \rho_0 \nu \frac{\partial u}{\partial z} \\ -\tau_\theta &= \rho_0 \nu \frac{\partial v}{\partial z} \end{aligned} \right\} \dots (6)$$

and

$$w|_{z=0} = 0,$$

where τ_λ and τ_θ are the components of wind stress in the λ and θ directions respectively. Since temperature and salinity equations are not included in the model equations, there is no need of giving surface boundary conditions for temperature and salinity.

At the bottom $z = H(x, y)$, a nonslip boundary condition for velocity fields was applied.

$$\text{i.e. } u = v = w = 0 \dots (7)$$

Along the lateral rigid boundaries, the normal flux boundary condition of zero velocity is prescribed.

$$\vec{V}_n = 0, \quad \dots (8)$$

where 'n' is the normal to the boundary.

Open Boundary Conditions

If observed data on flow fields at few stations along the open boundaries are available, those data could be interpolated to all grid points along the boundary and such data are the best for the specification of open boundary conditions. Since current meter observations along the southern and eastern open boundaries were not available, it has become necessary to compute the flow field across the boundaries by indirect method. There are a number of theoretical method to compute the flow field in the ocean and it is essential that the best method should be employed to obtain realistic values of current across the open boundaries. The theoretical method to compute the velocity fields should take into consideration the wind stress and thermohaline forcing. One of the drawbacks of geostrophic computation is that it computes only one component of the relative current that flows across the boundary. In addition, it also does not take into consideration the direct effect of wind stress which mainly controls the surface circulation. In view of this, we decided to use a quasi-geostrophic model developed by Marchuk and Sarkisyan³ to compute the velocity components at various levels along the southern and eastern open sea boundaries. This model takes into consideration wind stress, density field and sea level for the computation of velocity components. The original quasi-geostrophic model of Marchuk and Sarkisyan, written in cartesian co-ordinates, were converted into spherical co-ordinate system as our model equations are in spherical co-ordinate system. The modified quasi-geostrophic formulae for the computation of velocity components are:

$$U_{Qg} = \frac{g}{l} \left[\frac{1}{R} \frac{\partial \eta}{\partial \theta} + \frac{1}{\rho_0 R_0} \int^z \frac{\partial \rho'}{\partial \theta} dz \right] + \frac{e^{-\alpha z}}{2\rho_0 \alpha \nu} [(\tau_\lambda \pm \tau_\theta) \cos \alpha z - (\tau_\lambda \pm \tau_\theta) \sin \alpha z] \quad \dots (9)$$

$$V_{Qg} = -\frac{g}{l} \left[\frac{1}{R \sin \theta} \frac{\partial \eta}{\partial \lambda} + \frac{1}{\rho_0 R \sin \theta_0} \int^z \frac{\partial \rho'}{\partial \lambda} dz \right] + \frac{e^{-\alpha z}}{2\rho_0 \alpha \nu} [(\tau_\theta \pm \tau_\lambda) \cos \alpha z - (\tau_\theta \pm \tau_\lambda) \sin \alpha z], \quad \dots (10)$$

where $\alpha = [(\Omega \sin \phi) / \nu]^{1/2}$, the Ekman parameter of the ocean. The sea level η is computed by means of dynamic method. The sign (+) refers to northern hemisphere. To conserve volume/mass in multilevel, baroclinic, regional circulation models, the open boundary conditions are prescribed either in terms of volume fluxes or velocity fields. The normal sign convention used to balance the volume flux/velocity is that volume flux into the model area through the open boundary is taken as positive. The volume flux out of the model area is taken

as negative. Whatever may be the sign convention used in the model, these changes in sign convention will have to be made while calculating volume flux balance.

The zonal volume flux across the eastern open sea boundary is calculated using the formula:

$$F_E = - \int_{\theta_1}^{\theta_2} \int_0^H U_{Qg} dz d\theta, \quad \dots (11)$$

where θ_1 and θ_2 are the latitudinal extent of the open boundary and H is the depth of the model area.

The meridional volume flux across the southern open boundary is calculated using the formula:

$$F_S = - \int_{\lambda_1}^{\lambda_2} \int_0^H V_{Qg} \sin \theta dz d\lambda, \quad \dots (12)$$

where λ_1 and λ_2 are the longitudinal extent of the open boundary.

The total volume flux, ($F_T = F_E + F_S$), across the eastern and southern boundaries must be balanced to conserve volume in the model area. If the total volume flux across the southern and eastern boundaries are not balanced, we apply velocity fields as open boundary conditions, after making necessary correction to the velocity fields. It has been found that, while there is an approximate balance between the incoming and outgoing volume fluxes across the southern open sea boundary, these are not balanced across the eastern boundary because of the massive zonal fluxes into the model area from the system of zonal currents in the equatorial regions. In view of this, we applied corrected velocity fields as open boundary conditions. Velocity correction, V_c to every point in the open boundary considering total flux can be written as:

$V_c = F_T/A$, where A is the lateral surface area of the open boundary. This velocity correction was added to the quasi-geostrophic velocities computed by the formulae (9) and (10).

For the eastern boundary, the corrected u -component of quasi-geostrophic velocity is:

$$U_{Qg} = U_{Qg} + V_c \quad \dots (13)$$

For the southern open boundary, the corrected V -component of quasi-geostrophic velocity is:

$$V_{Qg} = V_{Qg} + V_c \quad \dots (14)$$

After having corrected the velocity at each grid point the balance of the normal component of quasi-geostrophic velocity (eqs 13 and 14) were again checked for the conservation of volume and it has been found that a velocity balance of

0.002 cm/sec was achieved across the open boundaries. The V -component of quasi-geostrophic velocity as computed by eq. (10) and the corrected zonal component of velocity as calculated by eq. (13) are applied at the eastern open boundary. At the southern open sea boundary, the u -component of quasi-geostrophic velocity as computed by eq. (9) and the corrected component of velocity as calculated by eq. (14) are applied.

Initial conditions. An initial state of rest is prescribed at time $t=0$ i.e. $(u, v)_{t=0} = 0$.

Derivation of Sea Surface Topography Equation

A detailed discussion on the various methods of derivation of sea surface topography equation is given in the works of Demin and Ibraev¹⁶. In the present paper, the equation for sea surface topography is derived in the following form:

The solution of eqs (1)-(4), considering equation for hydrostatic pressure (5), is obtained with the help of leap-frog numerical scheme mentioned above. By summing the equation of continuity along all levels taking into account the boundary condition at the surface and bottom for vertical velocity (i.e., $W=0$), the two dimensional integral continuity equation is obtained. The two-dimensional integral continuity equation is the equation for sea surface topography at the internal grid point. By applying the lateral boundary condition for velocity field in the two-dimensional integral continuity equation, the equation for sea surface topography at the solid boundary points (coastal) are also obtained. The two-dimensional integral continuity equation for sea surface topography at the internal grid points is written as follows:

$$\frac{1}{R \sin \theta} \left[\delta_{\lambda} \bar{u}^{\rho} + \delta_{\theta} \bar{v} \sin \theta^{\lambda} \right] = 0 \quad \dots (15)$$

where δ_{λ} and δ_{θ} are the finite difference operators and \bar{u} and \bar{v} are the vertically integrated velocity components in the zonal and meridional directions respectively. The finite difference operations δ_{λ} and δ_{θ} in the zonal and meridional direction respectively are defined as follows:

$$\delta_{\lambda} f = \left[f \left(\lambda + \frac{\Delta \lambda}{2} \right) - f \left(\lambda - \frac{\Delta \lambda}{2} \right) \right] / \Delta \lambda;$$

and

$$\delta_{\theta} f = \left[f \left(\theta + \frac{\Delta \theta}{2} \right) - f \left(\theta - \frac{\Delta \theta}{2} \right) \right] / \Delta \theta.$$

Substituting the values of \bar{u} and \bar{v} in the integral continuity equation, we get the expression for sea surface topography as follows:

$$\frac{1}{R \sin \theta} \left[\delta_\lambda \left[\frac{a \delta_\lambda \bar{\xi}^\theta + b \delta_\theta \bar{\xi}^\lambda}{4} \right]^\theta + \delta_\theta \left[\frac{a \delta_\theta \bar{\xi}^\lambda - b \delta_\lambda \bar{\xi}^\theta}{4} \right]^\lambda \sin \theta \right] = R_s, \quad \dots (16)$$

where

$$a = \frac{\Delta t g H}{1 + \frac{\Delta t^2 l^2}{4}}; \quad b = a l \frac{\Delta t}{2},$$

$$R_s = \frac{1}{R \sin \theta} \left[\delta_\lambda \bar{R}_\lambda^\theta + \delta_\theta \left(\bar{R}_\theta^\lambda \sin \theta \right) \right],$$

$$R_\lambda = R_u - \left(\frac{\Delta t l}{2} R_v \right) \left/ \left(1 + \frac{\Delta t^2 l^2}{4} \right) \right.,$$

$$R_\theta = R_v - \left(\frac{\Delta t l}{2} R_u \right) \left/ \left(1 + \frac{\Delta t^2 l^2}{4} \right) \right.,$$

$$R_u = u^{n-1} + \Delta t \left[\frac{-l v^{n-1}}{2} - \left(\frac{g}{\rho_0 R \sin \theta} \int_0^z \frac{\partial \rho''}{\partial \lambda} dz - A u - \cot \theta \frac{u v}{R} \right)^n + (F^\lambda)^{n-1} \right]$$

and

$$R_v = v^{n-1} + \Delta t \left[\frac{+l u^{n-1}}{2} - \left(\frac{g}{\rho_0 R} \int_0^z \frac{\partial \rho'}{\partial \theta} dz - A v - \cot \theta \frac{u^2}{R} \right)^n + (F^\theta)^{n-1} \right].$$

It is clarified that the model computed sea level (eq. 16) and the sea level required for calculating the quasi-geostrophic velocities (eqs 9 and 10) are different. The model computed sea level was not used for the calculation of sea surface topography at the open boundaries as the application of the same at the open boundaries will disturb the quasi-geostrophic balance maintained there. For all multilevel ocean models that involves sea level as an integral function, the above mentioned procedure has been used to conserve volume in the model area. The sea surface topography equations (eq. 16) has been solved by successive over relaxation technique. In fact, eq. (16) can be solved by any one of the iterative methods. While solving the above equation, the relaxation parameter used was 1.0. By using a relaxation parameter equal to 1.0, the successive over relaxation method will automatically convert itself to Gauss-Seidel iteration method. The convergence of the iterative solution was determined by numerical experiment and it has been found that the maximum residual, $\max |\xi^{n-1} - \xi^n| \approx 10^{-5}$ cm, where n is the iteration number, has been achieved after 100 iterations.

Model Forcing Parameters and Numerical Solution Procedure

To calculate the monthly mean circulation and sea surface topography using the above diagnostic model, monthly mean wind stress and monthly mean density anomaly (density) at various levels are required. The monthly mean wind data used in the present study come from Hellerman and Rosenstein¹⁷ who prepared the global wind stress field on a $2^\circ \times 2^\circ$ square. These data were further interpolated to 1° resolution, which is the spatial resolution of our model, by means of a bilinear interpolation technique. The monthly mean temperature and salinity data (density anomaly) needed to drive the model come from Levitus¹⁸. The monthly mean temperature data were available for all the 12 months; however, monthly mean salinity data were not available because salinity observations in the sea are few orders less than temperature observations. On a monthly scale, variations in salinity are observed in the second or third point only and such variations do not affect the calculation of density anomaly or mean currents. The diagnostic and semi-diagnostic circulation models are meant for the calculation of steady state circulation and it is not essential to mathematically interpolate the monthly mean salinity data from seasonal mean data for such models; however, in prognostic circulation models, which are intended for the study of time-dependent circulation, it is essential to interpolate mathematically the surface boundary condition for salinity at each time step of integration. Cox⁴ used annual mean salinity data as the surface boundary condition for all the 12 months without any mathematical interpolation, although the model was prognostic. It is fully justified in taking the same seasonal mean salinity data as the monthly mean salinity data for all those months representing that particular season. In the present study, the monthly mean salinity data for all the 12 months were obtained without interpolation from four season's salinity data which were compiled by Levitus¹⁸.

Model eq. (1-4), considering eq. (5) were solved subject to boundary and initial conditions mentioned above using a leap-frog numerical scheme. While the coriolis term is treated in a semi-implicit fashion, the friction terms are calculated at the backward time level. All the other terms in the equations are calculated at the central time level. To inhibit time-splitting instability normally encountered in leap-frog scheme, a Matsuno scheme, which averages solution at two conservative time steps was employed at every 24 time steps. Equations are integrated forward in time with a time step of 1 hour for approximately 25 days to attain a steady state solution. Solutions are found on staggered grid, with the variables defined in rectangular boxes of dimensions $\Delta X = \Delta Y = 1$ degree (Fig. 2). The velocity vector V is determined at the centre of the box. The model has 18 levels in the vertical at standard oceanographic depths. The horizontal and vertical eddy viscosity coefficients used in the model are $10^8 \text{ cm}^2/\text{sec}$ and $10 \text{ cm}^2/\text{sec}$ respectively. To calculate the January mean circulation and sea surface topography, the model is to be driven with January mean density anomaly and January mean wind field as forcing parameters, and the corrected quasi-geostrophic velocity as calculated by equations (13) and (14) for the month of January as open boundary conditions. The steady state circulation, which is obtained after 25 days of model integration, is the monthly mean circulation for

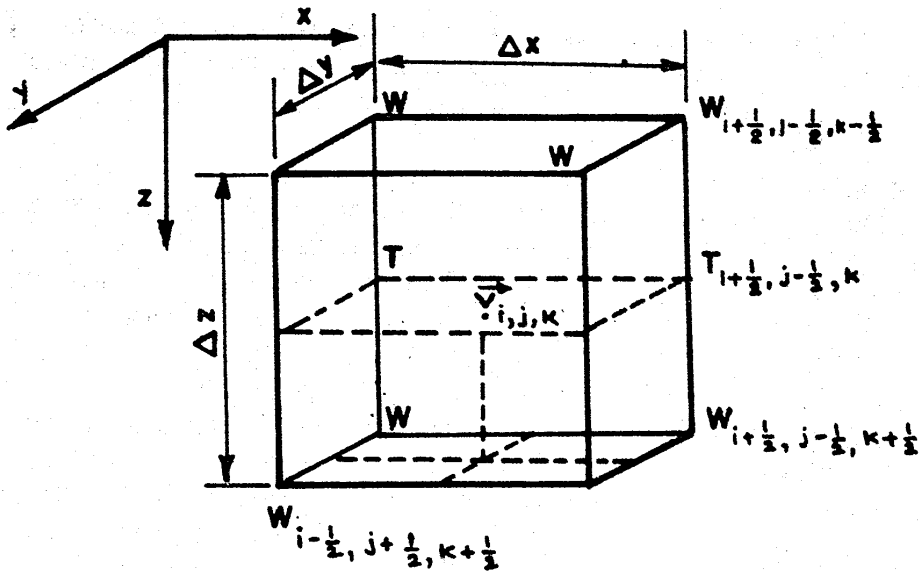


Fig 2 A typical box in the finite-difference grid

the month of January. Using appropriate boundary conditions and model forcing parameters for each month, the mean circulation and sea surface topography for all the 12 months were computed by conducting 12 numerical experiments. It is clarified that, for each month, the corresponding open boundary conditions are to be specified.

Results and Discussion

Variability of Monthly Mean Sea Surface Topography and Its Associated Circulation

Sea surface topography is a dynamic variable intimately linked to the flow fields in the upper mixed and thermocline layers. While the upper mixed layer circulation is essentially controlled by the resultant of wind stress and sea surface slope, the circulation in the thermocline is mainly determined by sea surface topography (sea level). The slope of the sea surface affects the slope of the thermocline which, in turn, affects the thermocline circulation. Both the surface wind stress and interior flow fields are responsible for generating sea surface slope. Oceanic motions occurring in the main thermocline and above on spatial scales exceeding the Rossby radius of deformation will penetrate vertically to the surface and generate pressure signals which are reflected in the form of sea surface slope. The magnitude of sea surface slope depends on the time and space scales of motions that are occurring within the oceanic thermocline and above. Of all the strong components of time-averaged circulation, the types of circulation that are indeterminate through sea surface topography are the deep western boundary currents. Features such as gross thermocline shape, powerful surface boundary currents and strong tropical circulation patterns are reflected in the sea surface topography. In the present paper, we discuss the computed results of sea surface topography for all the 12 months and bring out

the characteristics of surface circulation associated with the sea surface topography. Results of 3-dimensional circulation in relation to all the model forcing parameters will be presented in our future papers.

(a) January Mean Sea Surface Topography

The topography of sea surface (SST) for the month of January, calculated with the help of eq. (16), is presented in Fig. 3a. In the southern part of Tropical Indian Ocean between 20°S and 10°S latitude, a zonally oriented ridge with steep equatorward downward slope that extends across the entire basin was observed in January. There is strong packing of topography contours in the ridge region, indicating that currents at this region would penetrate deeper into thermocline and below. This ridge region is the domain of the south equatorial current which does not vary much during different seasons. Few contours of surface topography from the south equatorial current turn toward north and northeast on approaching the East African coast. These north and northeasterly topographic contours along the East African coast represent the East African Coastal Current (EACC) which flows northeast during the winter season. The EACC of the southern hemisphere and the Somali current (SC) of the northern hemisphere meet south of Equator and both jointly feed the Equatorial Counter Current (ECC). The topography contour gradients are relatively weak across EACC and Mozambique Current (MZC). In the north western part of the basin north of 15°N latitude and along the west coast of India, the flow field is generally northerly consistent with ship drift climatology. The computed sea surface topography fully agrees with the dynamic topography calculated by Hastenrath and Greischar²⁴.

(b) February Mean Sea Surface Topography

The sea surface topography for the month of February is presented in Fig. 3b. The sea surface topography pattern did not vary much as compared to January month except that intensity of topography gradients decreased slightly in February. As in the month of January, the topography contours are well packed in SEC and North Madagascar Current region (NMC). The topography contours show the presence of SEC, NMC, MZC, ECC and EACC in the southern tropical Indian Ocean. Another change noted is that flow field is on-shore off northern Somali coast in February, compared to south westerly flow observed during the preceding month. Northerly and northwesterly flows are observed along the west coast of India and it is expected that this current may penetrate deeper into the thermocline because of the comparatively high topography gradient existing in this region. These results are consistent with the ship drift climatology compiled by Cutler and Swallow¹⁹.

(c) March Mean Sea Surface Topography

The sea surface topography for the month of March is presented in Fig. 3c. As in the previous month, there are hardly any changes in sea surface topography pattern in the SEC region which is under the influence of southeast trade winds throughout the year. The sea surface contours slope upwards toward the coasts of Mozambique and East Africa due to the piling up of water

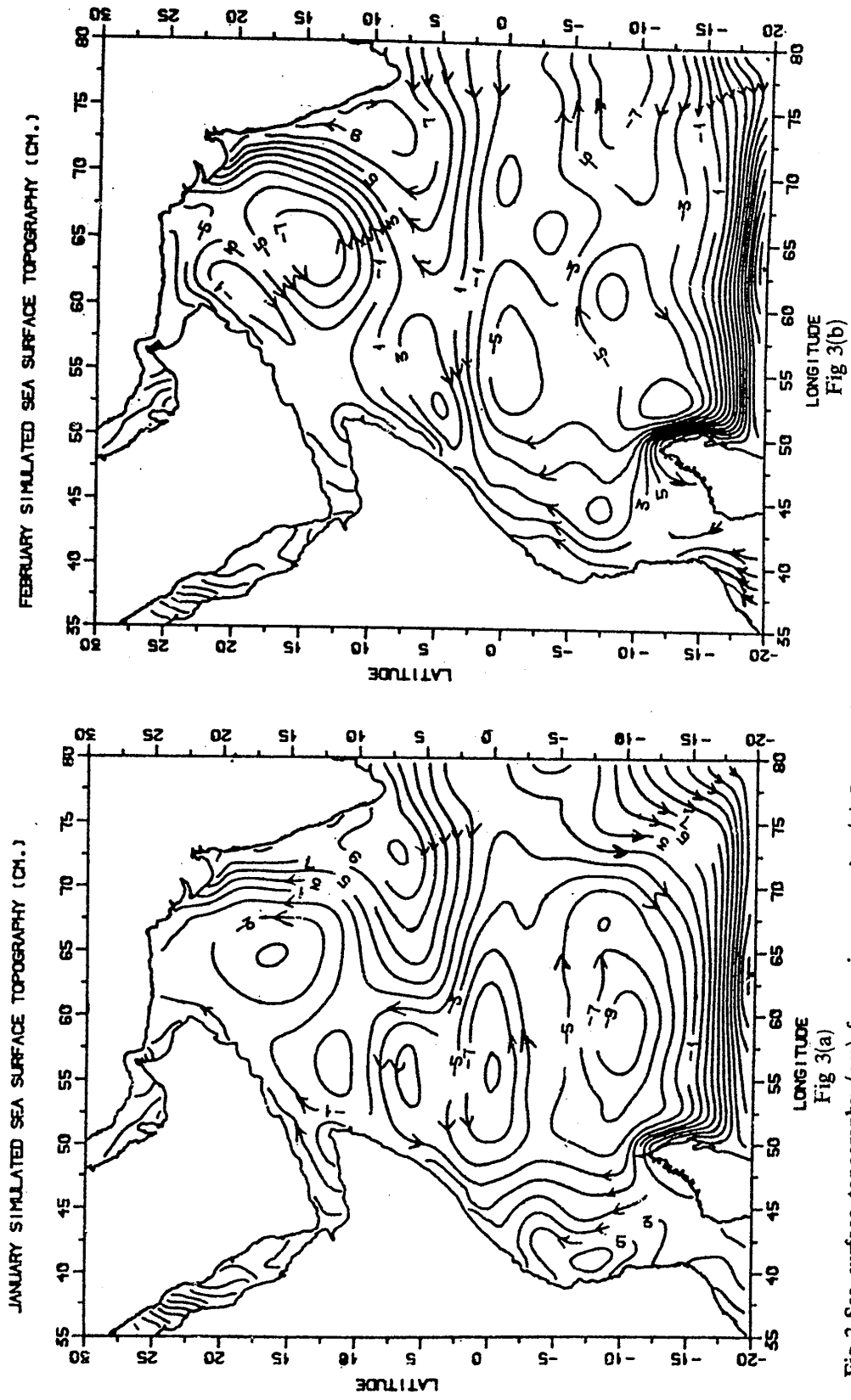


Fig 3 Sea surface topography (cm) for various months: (a) January (b) February (c) March (d) April (e) May (f) June (g) July (h) August (i) September (j) October (k) November (l) December.

under the influence of prevailing southeasterly trades. The Ekman wind-driven current, resulting from the prevailing southeasterly trades, is primarily directed toward south of west and it results in the formation of a permanent ridge throughout the year around 15°S latitude. The geostrophic surface current due to the presence of this ridge is also directed towards south of west, although it is very much smaller than surface Ekman current. The SEC is, therefore, both wind-driven and geostrophic. The ECC, observed in February, is still prevalent between 10° and Equator across the entire basin. However, currents in the northern Indian Ocean is slightly modified in comparison with February month pattern. The current direction off the northern Somali coast is reversed and the Somali current flows in a northeasterly direction. The north equatorial current is weakened, flows towards west only upto the central part of Arabian Sea and then turns toward northeast. The flow field in the entire northwestern Arabian Sea is toward northeast probably due to the collapse of northeasterly trade winds during the month of March.

(d) April Mean Sea Surface Topography

The computed sea surface topography for the month of April is presented in Fig. 3d. During April, northeasterly winds are very much weakened in the northern Indian Ocean. The most dramatic circulation feature during April is the appearance of an eastward flowing Equatorial Jet (EWJ) under the influence of westerly winds. It has been found that the sea surface slopes upward toward the eastern boundary of the model basin (Fig. 3d) under the influence of westerly winds. The sea surface topography contours show the presence of a large clockwise gyre in the southern Tropical Indian ocean, with south equatorial current on the south, east African Coastal Current on the west and Equatorial jet on the north. In the northern Arabian Sea, the flow field is northerly and northeasterly. The simulated sea surface topography pattern during April is consistent with observed surface circulation in the Tropical Indian Ocean during the transition season.

(e) Mean Sea Surface Topography for the Month of May

The computed sea surface topography for the month of May is presented in Fig. 3e. During May, the southeast trades of the southern hemisphere become stronger, approach the equator and become southwesterly over the Somali and Arabian coasts. Under the influence of strong southerly and southwesterly winds, waters are piled up against East African and Somali coasts, creating strong northerly and northeasterly flows along its coasts. The sea surface topography pattern, as calculated by the model, clearly shows the presence of strong currents in these regions. The topography contours are highly packed in the south equatorial current and East Madagascar current regions as in the previous months. The meridional gradient in the sea surface topography that existed in the southern tropical Indian Ocean in the previous month has further deepened with the strengthening of southeast trade winds. In addition, the south equatorial current becomes very much broader in response to strong southeast trade winds. The Somali current, which is the northward extension of the East

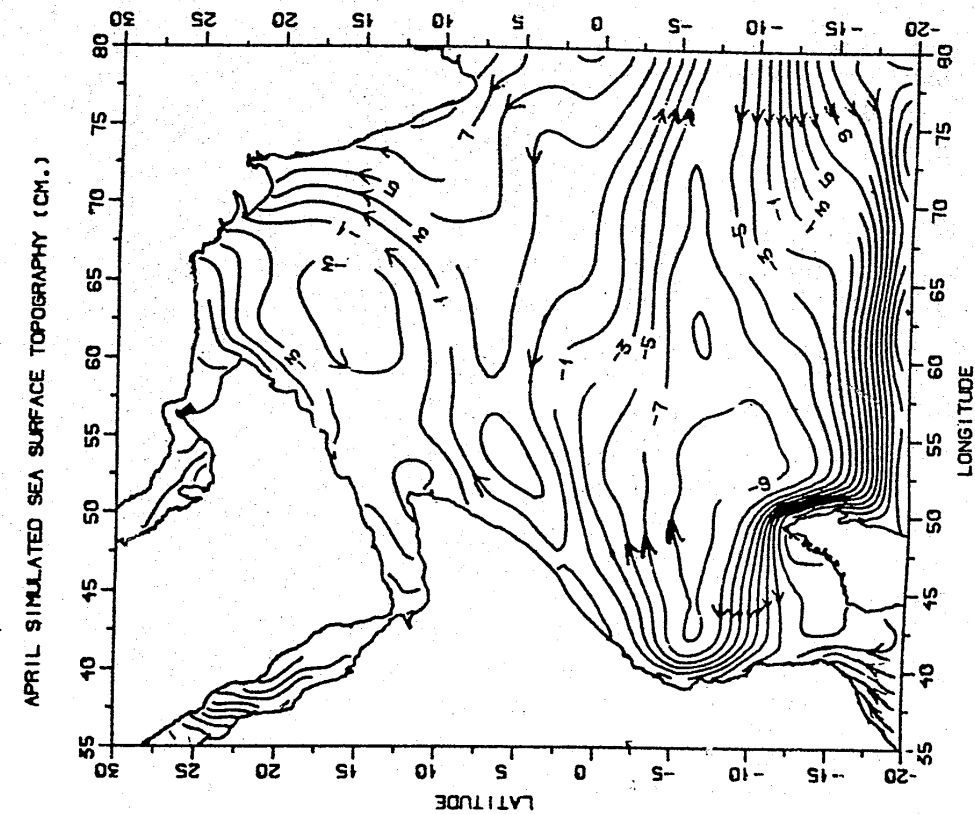


Fig 3(d)

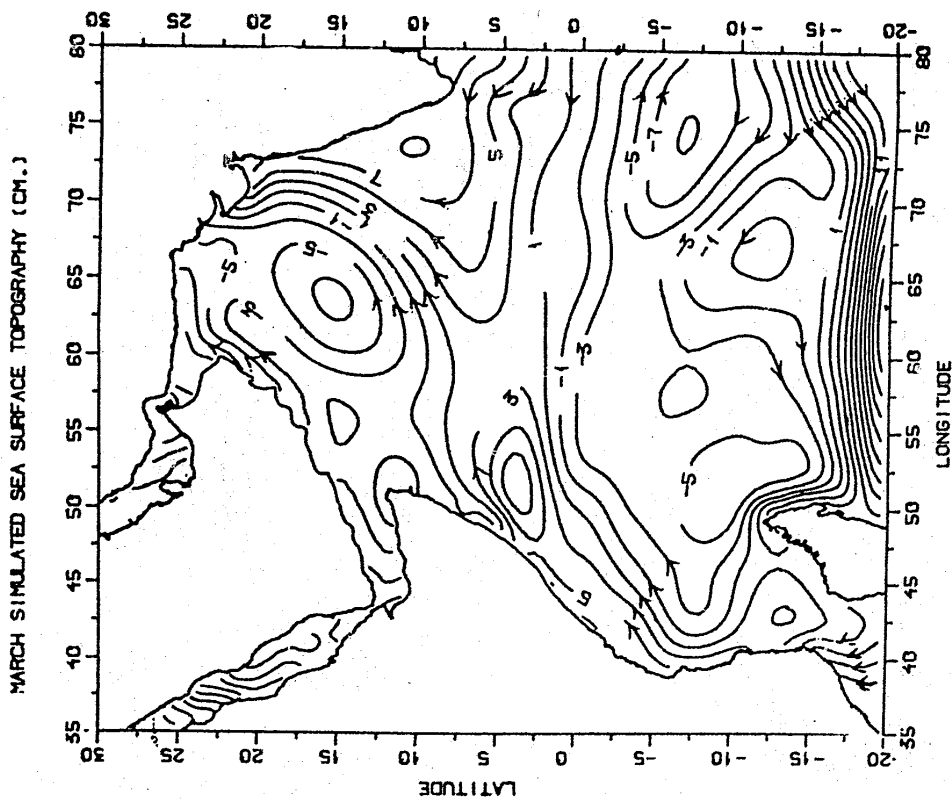


Fig 3(c)

(Please see Caption details on Page No. 337)

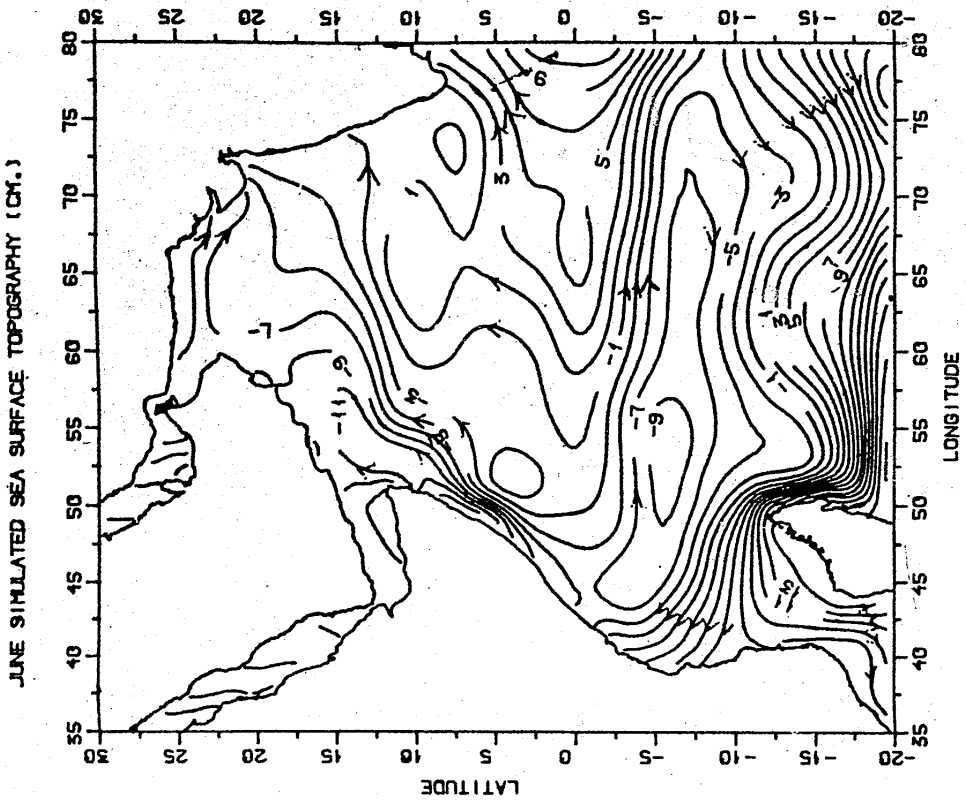


Fig 3(f)

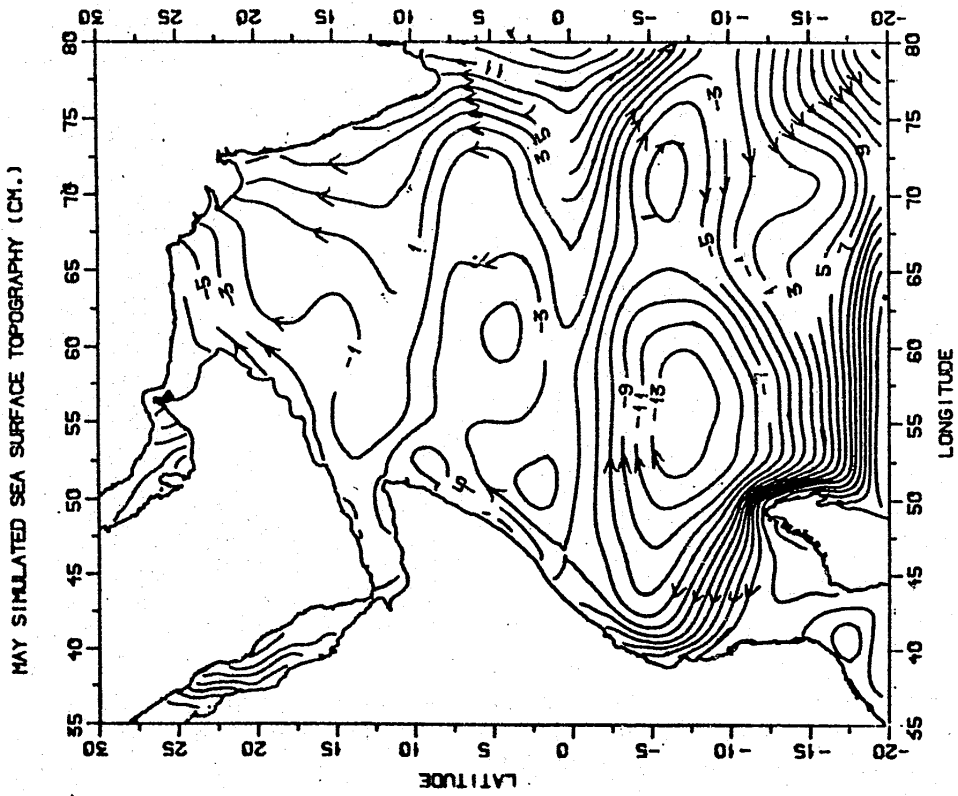


Fig 3(e)

(Please see Caption details on Page No. 337)

African Current, is well established during the month of May. Consistent with the dynamics of the model the sea level is low along the Somali coast due to strong offshore Ekman transport. Both the sea level slope and wind field are favourable for the generation of strong current along the Somali coast.

(f) Mean Sea Surface Topography for the Month of June

During the month of June, the southwest monsoon is fully set over the entire tropical Indian Ocean. The sea surface topography contours (Fig. 3f) are more packed along the coasts of Somalia, indicating that Somali current is further strengthened with the onset of monsoon winds over the north Indian Ocean as compared to the previous month. The sea surface topography contours show northerly and northeasterly flows in the entire northern Indian Ocean consistent with the observed flow pattern. A weak equatorial counter current is observed between the equator and 7° south latitude. In the southern tropical Indian ocean, the meridional sea surface topography gradient found in the SEC is slightly weakened probably due to the weakening of southeast trades. However, there is a strong packing of topography contours along the eastern coast of Madagascar. Another change noted in the southern tropical Indian Ocean is the presence of a southward flow along the coast of Mozambique. In general, the calculated sea surface topography pattern is fully consistent and comparable with the observed circulation features during summer season.

(g) July Mean Sea Surface Topography

The computed sea surface topography pattern for the month of July (Fig. 3g) not very much different from that of June months simulation results except that the zonal topography gradient found off Somali and Arabian coasts are strengthened a little more. It shows that currents along the Somali and Arabian coasts became still stronger in July. The southwest monsoon drift current occupies the entire western Arabian sea. In addition, the flow along the southwest coast of India has become more southerly consistent with observed circulation features. The broad south equatorward current, north Madagascar current, East African Coastal Current and the Equatorial Counter Current observed during the preceding month are found during the month of July also.

(h) Mean Sea Surface Topography for the Month of August and September

The sea surface topography for the months of August and September are presented in Figs 3h and 3i respectively. All the current systems that are found during the month of July are observed during August also. However, the intensity of current is slightly weakened in the whole model area probably due to the weakening of monsoon winds during August and September. The topography contours and the flow field along the west coast of India have become more southerly and southeasterly.

(i) Mean Sea Surface Topography for the Months of October and November

The computed sea surface topography for the months of October and November are presented in Figs 3j and 3k respectively. During these transition

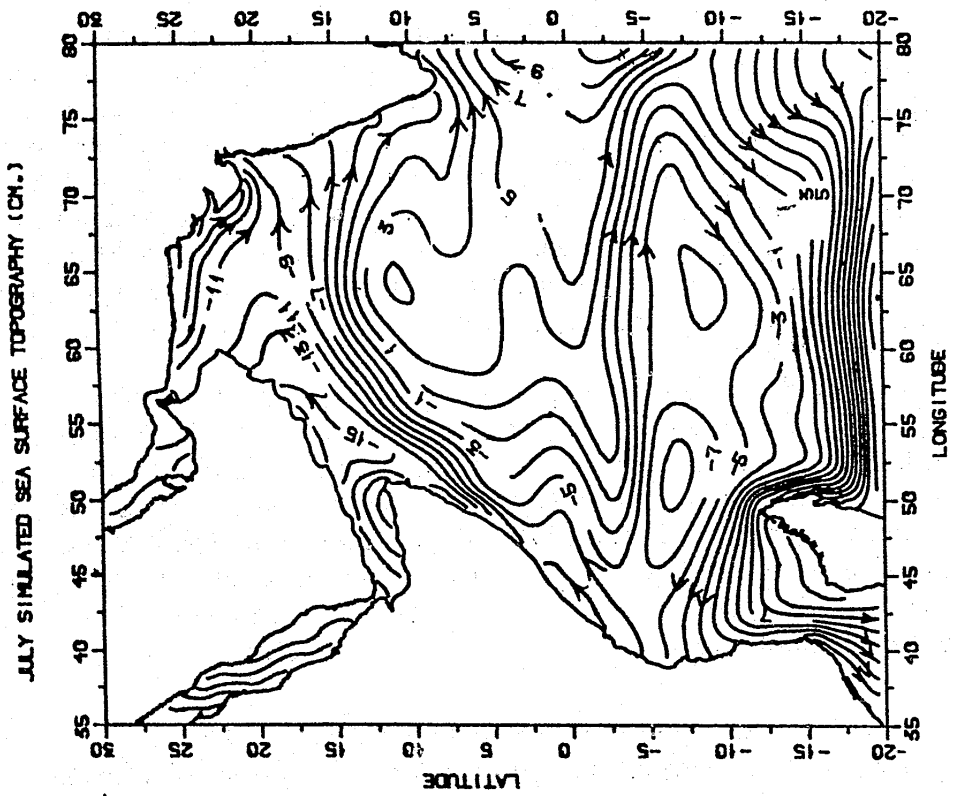
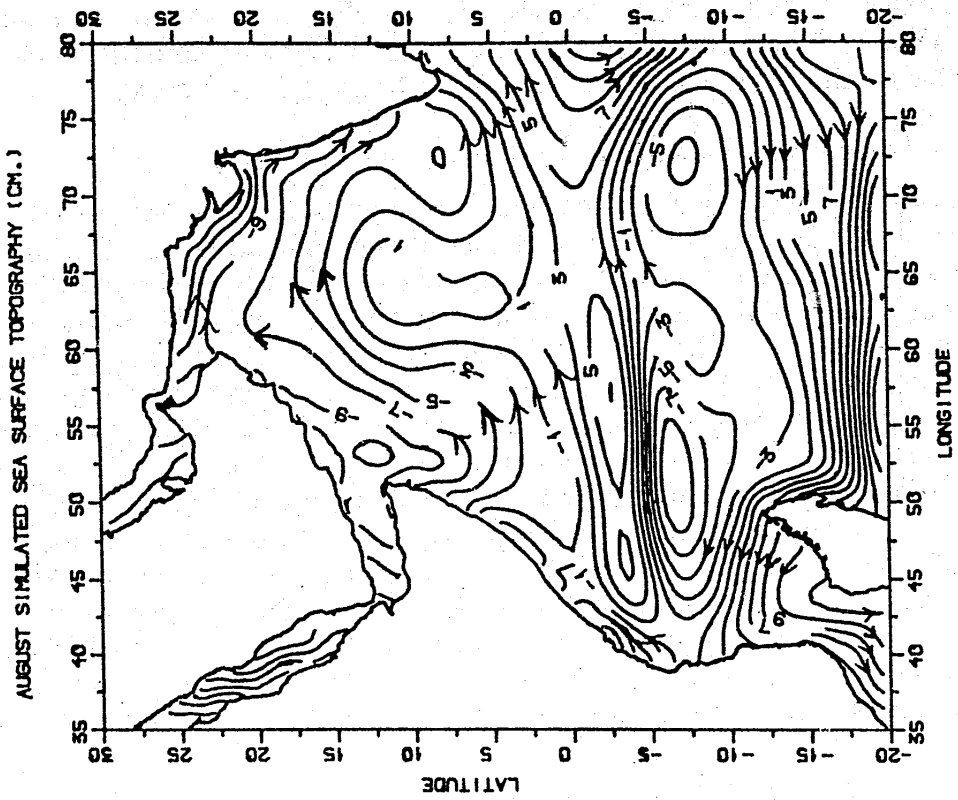


Fig 3(h)

Fig 3(g)

(Please see Caption details on Page No. 337)

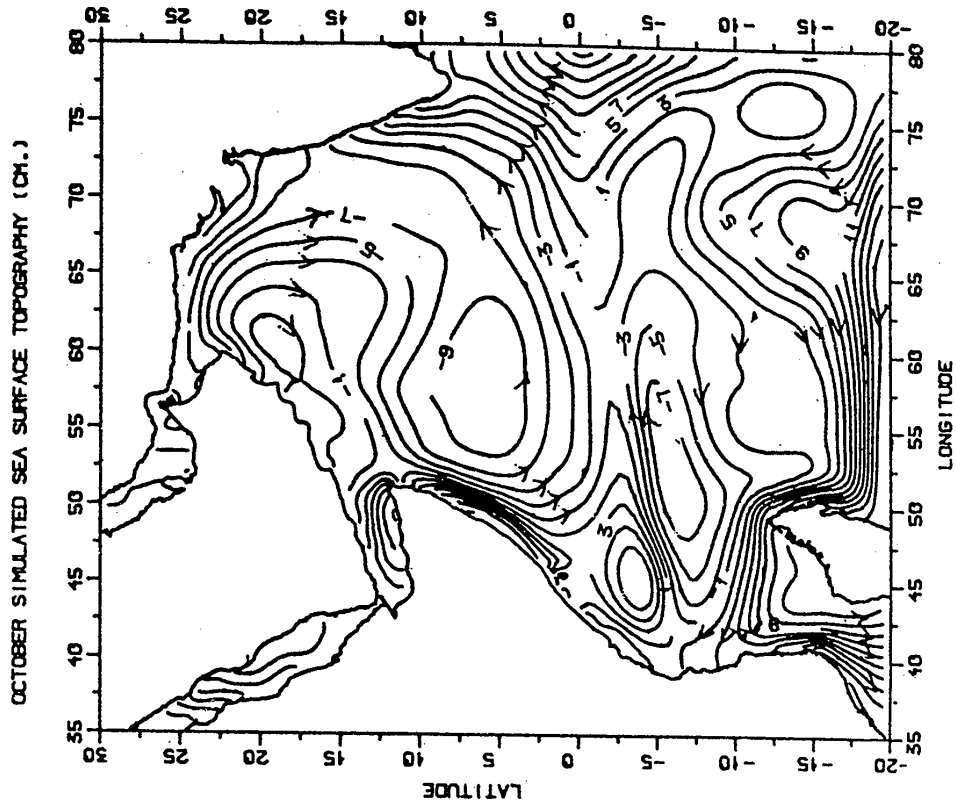


Fig 3(j)

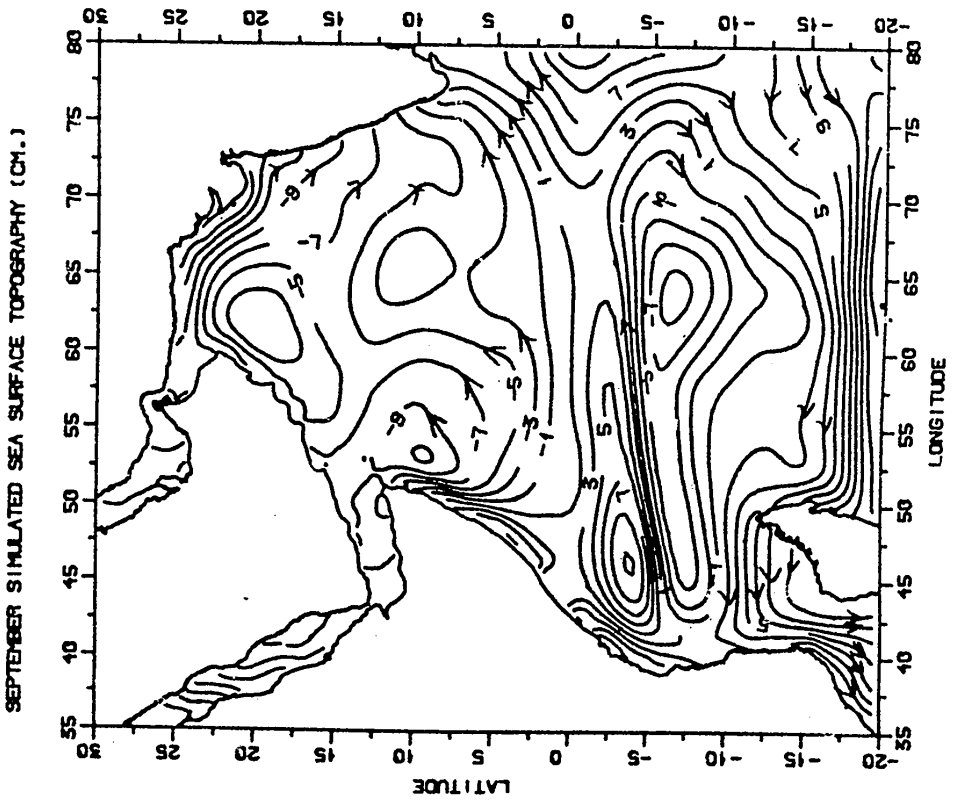


Fig 3(i)

(Please see Caption details on Page No. 337)

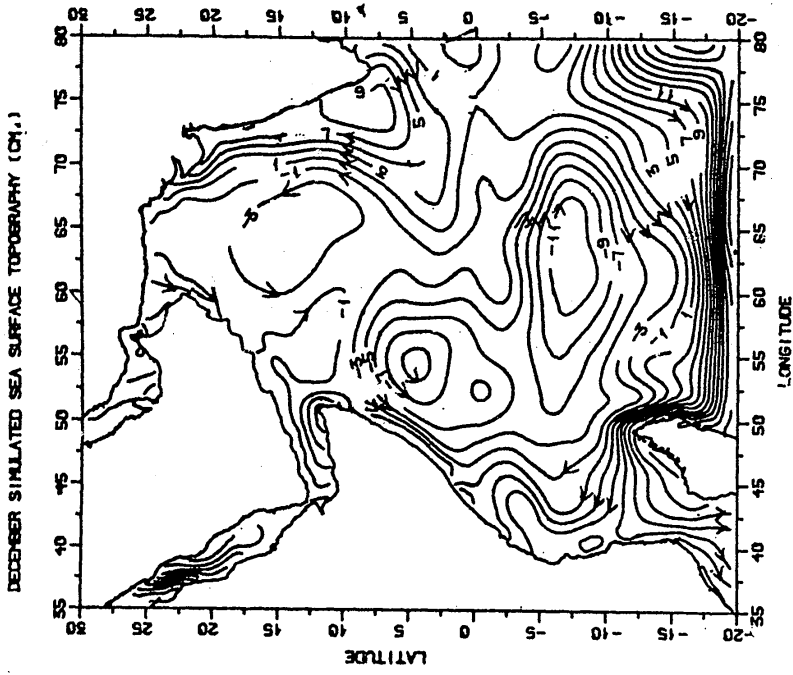


Fig 3(l)

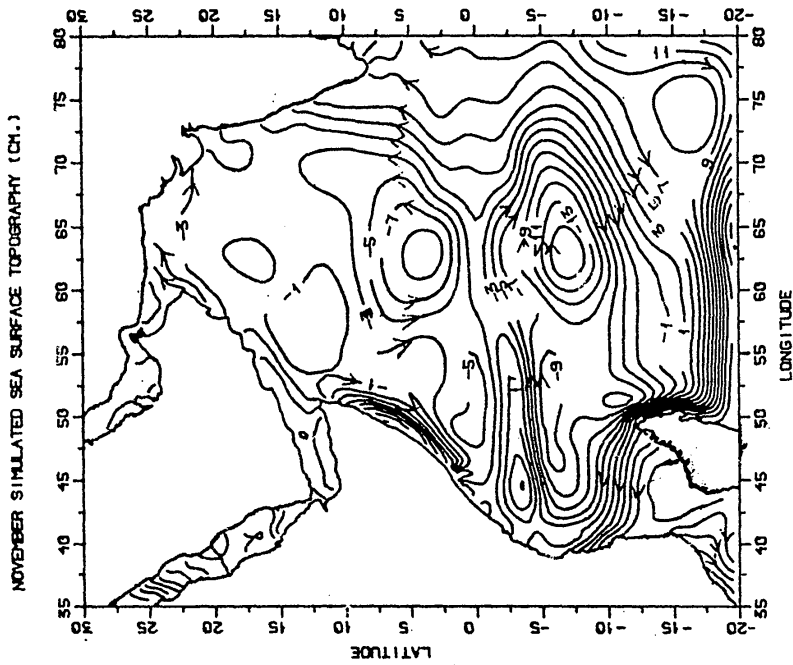


Fig 3(k)

(Please see Caption details on Page No. 337)

months, the circulation features are almost identical to that observed during the spring season. The most significant feature of circulation is the appearance of eastward flowing equatorial jet near the Equator which is mainly fed by the south equatorial current and Somali current. The eastward flowing equatorial jet was observed in both the months of October and November. The Somali current now flows southwestward all along the coasts and feeds the equatorial jet. The flow pattern in the entire northern Arabian Sea is changed, with southward and southwestward flows observed throughout the Arabian Sea. In the southern Tropical Indian Ocean, there are hardly any changes in the circulation pattern when compared to previous months. Currents such as SEC, EMC and MZC are found during these transition months also.

(j) Mean Sea Surface Topography for the Month of December

The sea surface topography contours for the month of December (Fig. 31) are almost identical to that of January month's topography. In December, which is the representative month of winter season, northeast monsoon winds sweep the northern Indian Ocean. In association with the northeast monsoon winds, the flow field is southerly and southwesterly in the western Arabian Sea. The sea surface topography pattern shows the presence of southward flowing Somali current along the coast of Somalia. As in the month of January, the topographic contours are almost parallel to the west coast of India and a fairly strong northward flowing coastal current is observed along the West Coast of India. The north equatorial current which flows westward between the equator and 8°N latitude, can be identified from the sea surface topography pattern. In the southern tropical Indian Ocean, sea surface topography contours show the presence of all the three major currents consistent with available observations.

Conclusions

(i) Diagnostic method has been found to be very effective for the calculation of sea surface topography in the Western Tropical Indian Ocean. Since the density is imposed on the model from observation of temperature and salinity, the spin up time of the model is very fast as compared to prognostic ocean models and the solution attains stationarity within 25 days of model integration.

(ii) Special care should be taken to prescribe the appropriate open boundary conditions in regional 3-d circulation models. While prescribing the open boundaries, it is to be ensured that either the normal volume flux or the normal components of velocities are balanced to conserve volume in the model area. As far as possible, meridional open boundaries should be avoided for the Indian ocean models since zonal fluxes are very massive in the equatorial regions of Indian Ocean.

(iii) The diagnostic model has been successful for the calculation of sea surface topography for all the 12 months. The computed sea surface topography and its associated circulation are consistent with available observations on currents in the tropical Indian Ocean. In the southern tropical Indian Ocean south of 10°S

latitude, the computed sea surface topography patterns do not show much variability from month to month. This is mainly due to the absence of seasonal variability in the wind field. Monthly variability of sea surface topography was noted in the entire model area north of 10°S latitude.

(iv) The computed sea surface topography showed the presence of all the major permanent current systems in the model area for all the four seasons. However, the transient features of circulation such as eddies and small gyres, which are observed along the African coast during summer season, could not be reproduced by this diagnostic model. To simulate such transient features of circulation, it is essential to develop a prognostic model with which the time-dependent evolution of circulation in relation to time varying surface boundary forcings are studied. In diagnostic models, only the stationary circulation in response to constant local forcings of wind and density gradients were studied, and such a model might not always be successful in reproducing all the major and transient systems of currents in the Indian Ocean because of its time-dependence. Diagnostic models are effective tools to understand the forcing functions that control the dynamics of circulation and to determine the 3-dimensional climatic (mean) circulation. One of the main drawbacks of the diagnostic model is that the observed input of density field at various levels is not hydrodynamically adjusted with the flow field, wind field and bottom topography; the observed density field, which is not hydrodynamically adjusted, may generate unrealistic geostrophic flows and such unrealistic flows are normally observed in the equatorial region where geostrophy fails. By reducing the space scale of the model near the equator and applying higher values of horizontal friction coefficients, realistic flow pattern can be obtained from diagnostic model.

Acknowledgements

Authors are grateful to the Director NIO and the Head, Physical Oceanography Division for encouragement and providing necessary facilities. Authors are also indebted to one anonymous reviewer who gave constructive suggestions to improve the quality of this paper. The entire computational works were carried out at the Avion-4000 computer at the data division of this institute and the assistance and cooperation offered by the staff of the division are gratefully acknowledged. Authors are also grateful to DST, New Delhi, for granting a project under the TOGA-1 Modelling Programme under which the present work was carried out.

References

- 1 Yu L Demin and A S Sarkisyan *J mar Res* 35 (1977) 2 339
- 2 A S Sarkisyan *The Sea: Marine Modelling* (Eds E D Goldberg *et al*) J Wiley, New York (1977) 363-458
- 3 G I Marchuk and A S Sarkisyan *Mathematical Modelling of Ocean Circulation* Springer-Verlag Berlin (1988), p 292
- 4 M D Cox *Deep Sea Res* 17 (1970) 47
- 5 M D Cox *Deep Sea Res* 23 (1976) 1139
- 6 M D Cox *J phys Oceanogr* 9 (1979) 511

- 7 D L T Anderson and D W Moore *Deep Sea Res* **26** (1979)
- 8 J P McCreary and P K Kundu *J mar Res* **46** (1988) 25
- 9 M E Luther and J J O'Brien *Progr Oceanogr* **14** (1985) 353
- 10 J C Kindle and J D Thompson *J geophys Res* **94**(C4) (1989) 4721
- 11 K E Woodberry, M E Luther and J J O'Brien *J geophys Res* **94** (1984) 17985-18002
- 12 C Perigaud and P Delecluse *Ocean-Air Interactions* **1** (1989) 289
- 13 J G Jenson *J geophys Res* **96** (1991) 22151
- 14 P K Das, S K Dube and G S Rao *Proc Indian Acad Sci (Earth and Planet Sci)* **96** (1987) 279
- 15 A E Gill *Atmosphere-Ocean Dynamic* Academic Press (1982) p 662
- 16 Yu L Demin and R A Ibraev *Sov J Numer Anal math Modelling* **4** (1989) 211
- 17 S Hellerman and M Rosenstein *J phys Oceanogr* **13** (1983) 1093
- 18 S Levitus *Climatological Atlas of the World Ocean NOAA Prof Pap* **13** US Government Printing Office (1982) p 173
- 19 A N Cutler and J C Swallow *Surface Currents of the Indian Ocean (to 25°S 100°E)* Computed from Historical Data Archived by Meteorological Office, Broadchell UK Institute of Oceanographic Sciences, Rep No 187 (1984) p 81
- 20 Fugio Shinzon and Norihisa Imasato *J geophys Res* **96**(1) (1991) 759
- 21 F Schott *J geophys Res* **91**(C) (1986) 10581
- 22 F Schott, J C Swallow and M Fieux *Deep Sea Res* **37** (1990) 1825
- 23 J C Swallow, R L Molinari, J G Bruce, O B Brown and R H Evans *J phys Oceanogr* **13** (1983) 1368
- 24 S Hastenrath and L Greischar *J geophys Res* **96**(C7) (1991) 12619